Local density of states at zigzag edges of carbon nanotubes and graphene

Ken-ichi Sasaki,* Kentaro Sato, and Riichiro Saito

Department of Physics, Tohoku University, Sendai 980-8578, Japan
and CREST, JST, Sendai 980-8578, Japan

Jie Jiang

Department of Physics, North Carolina State University, Raleigh, North Carolina 27695, USA

Seiichiro Onari and Yukio Tanaka

Department of Applied Physics, Nagoya University, Nagoya 464-8603, Japan

The electron-phonon matrix element for edge states of carbon nanotubes and graphene at zigzag edges is calculated for obtaining renormalized energy dispersion of the edge states. Self-energy correction by electron-phonon interaction contributes to the energy dispersion of edge states whose energy bandwidth is similar to phonon energy. Since the energy uncertainty of the edge state is larger than temperature, we conclude that the single-particle picture of the edge state is not appropriate when the electron-phonon interaction is taken into account. The longitudinal acoustic phonon mode contributes to the matrix element through the on-site deformation potential because the wave function of the edge state has an amplitude only on one of the two sublattices. The on-site deformation potentials for the longitudinal and in-plane tangential optical phonon modes are enhanced at the boundary. The results of local density of states are compared with the recent experimental data of scanning tunneling spectroscopy.

I. INTRODUCTION

The local electronic property near the edge of graphene depends on the lattice structure of the edge. For example, the zigzag edge induces edge states which are π-electron states localized near the edge while the armchair edge does not.[1] The edge states which have a flat energy dispersion show a peak in local density of states (LDOS) near the Fermi energy. The peak structure in LDOS has been observed at step edge of the zigzag type on a surface of graphite by scanning tunneling microscopy (STM) and spectroscopy (STS).[2–5] The LDOS peak is a direct evidence of the edge states because the peak is not observed at an armchair edge and the height of the peak decreases with increasing the distance of the STS tip on graphene plane from the zigzag edge. The data on LDOS are useful in understanding the energy and lifetime of an electron in the edge states. The lifetime of the electron is determined by electron-phonon (el-ph) interaction, and the el-ph interaction is important for almost flat energy dispersion when the Debye energy ($\hbar\omega_D \approx 0.2$ eV) is comparable to the energy bandwidth. Thus, the el-ph interaction for edge states affects STS spectra and is essential for an analysis of STS. In this paper, we consider self-energy correction for edge states induced by the el-ph interaction and compare the theoretical results of LDOS with experimental data.[2–4]

A complete flat energy dispersion relation of the edge states is widely recognized by the theory.[1] However, STM/STS[2–5] and angle-resolved photoemission spectroscopy[6] (ARPES) show that the edge states have a small but finite energy dispersion. Using STM/STS at graphite edge, Niimi et al.[2,3] and Kobayashi et al.[4,5] independently observed a peak in the LDOS below the Fermi energy by 20–30 meV. The peak position relative to the Fermi point

($E_F = 0$) shows that the edge states have a finite bandwidth. Using ARPES, Sugawara et al.[6] observed the Fermi surface of Kish graphite and found a weakly dispersive energy band near the Fermi energy. In the previous paper, we pointed out that next-nearest-neighbor (nnn) tight-binding Hamiltonian $\mathcal{H}_{nnn}$ is essential for the bandwidth.[7] As shown in Sec. II, $\mathcal{H}_{nnn}$ lowers the energy dispersion of the edge states as $E(k) = \gamma_n(2\cos ka + 1)$ $(2\pi/3 < ka < 4\pi/3)$, where γ_n and a are the hopping integral between nnn sites ($\gamma_n \sim 0.3$ eV) and a lattice constant of graphite ($a = 2.46$ Å), and the value of γ_n is calculated on the basis of density-functional theory by Porezag et al.[8] Since $ka = \pi$ state is located at the bottom of the band and $ka \rightarrow 2\pi/3$ (or $4\pi/3$) is located at the top of the band, the bandwidth of the edge states, W, is given by $W = \gamma_n$. However, the observed energy bandwidth (20–30 meV) is much smaller than γ_n. The reason why the observed bandwidth is smaller than γ_n is that the self-energy correction $\Sigma(k)$ renormalizes $E(k)$ as $E(k) + \text{Re}(\Sigma(k))$. Because the el-ph interaction makes the effective mass of the edge states large, W generally decreases by taking account of el-ph interaction. It is also noted that $\Gamma(k) \equiv -2\,\text{Im}(\Sigma(k))$ represents the energy uncertainty of the edge state. Since the Fermi-Dirac distribution function has a width of $k_B T$ around the Fermi energy (E_F), if $\Gamma(k) > k_B T$, then it is not appropriate to treat the edge state by a single-particle picture.

The el-ph interaction is calculated by the matrix element of deformation potential. When the wave function is expanded by tight-binding orbitals, the matrix element consists of on-site and off-site atomic deformation potentials.[9] The el-ph matrix element of a given wave function is defined by the sum of atomic deformation potentials over all carbon sites on which the electronic wave function has an amplitude. The el-ph interaction for edge states shows a different

behavior from that for extended states. The unit cell of graphene consists of two sublattices, A and B. The extended states have a finite densities on both sublattices, while the edge states have density only on one sublattice.[1] Suzuura and Ando pointed out for the extended states that the on-site atomic deformation potentials at A atom and B atom cancel each other out in the matrix element for a backward scattering process because of a phase difference of the wave functions for two sublattices.[10] Thus, only the off-site atomic deformation potential that is generally weaker than the on-site one contributes to the backward scattering. This is consistent with the fact that a metallic carbon nanotube (CNT) shows the quantum conductance and ballistic character at a low temperature.[11–13] However, the cancellation of on-site deformation potential does not occur for the edge states, since the wave function has an amplitude only on a sublattice for the edge state. Thus, we can expect a relatively strong el-ph interaction for the edge states and a large self-energy correction to the edge states.

The el-ph interaction for the edge states is relevant to many observations in experiment of CNTs. Superconductivity in CNTs is an important example. Takesue *et al.*[14] observed a drop of resistivity in multiwalled CNTs and pointed out that the connection of multiwalled CNTs to Au electrode is sensitive to the occurrence of the resistivity drop. Since the edge states enhance LDOS near the ends of a CNT, the el-ph interaction should be sensitive to the properties at the interface between the CNT and an electrode. Furthermore, we propose that the large LDOS and a strong el-ph interaction favor superconducting instability for the edge states.[15] The self-energy correction is important for an estimation of the superconducting transition temperature. Thus, a quantitative discussion of the el-ph interaction for edge states will play a decisive role for a future work on STS and superconductivity of graphene based materials.

This paper is organized as follows. In Sec. II, we give a method for calculating el-ph interaction for edge states. In Sec. III, we show phonon mode and localization length dependence of el-ph interaction. In Sec. IV, we calculate self-energy correction to edge states, by which we obtain a renormalized energy dispersion relation and LDOS. The theoretical results are compared with the experiment. Discussions and summary are given in Sec. V.

II. ELECTRON-PHONON INTERACTION FOR EDGE STATE

A. Edge states

The edge states of graphene are π-electronic states localized near the zigzag edge [Fig. 1(a)].[1] Since a CNT is a rolled-up sheet of graphene, the edge states may exist near the open boundaries of $(n,0)$ zigzag CNT regardless of the value of n [see Fig. 1(b)]. The energy eigenequation of the nearest-neighbor (nn) tight-binding Hamiltonian $\mathcal{H}_{\mathrm{nn}}|\Psi_k\rangle = E(k)|\Psi_k\rangle$ gives a flat energy band, $E(k)=0$, for the edge states where k is the wave vector along the edge. As shown in Fig. 1(c), the edge state (flat energy band) exists when $2\pi/3 < ka < 4\pi/3$ and $\mathcal{H}_{\mathrm{nnn}}$ lowers the energy dispersion of the edge states as $E(k)=W(2\cos ka+1)$ $(2\pi/3 < ka$
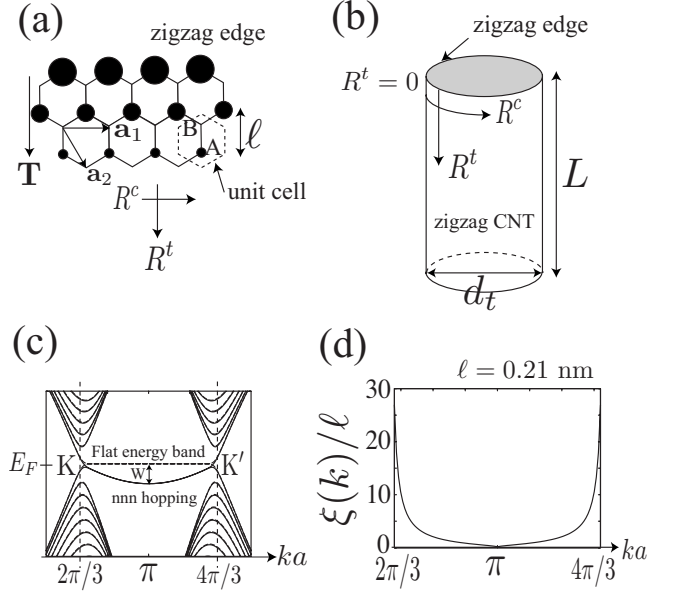
FIG. 1. (a) The unit vectors of graphene are denoted by $\mathbf{a}_1$ and $\mathbf{a}_2$. $\mathbf{a}_1$ is the unit vector around the tube axis and $\mathbf{T}(\equiv 2\mathbf{a}_2-\mathbf{a}_1)$ is the translational vector along the zigzag tube axis. We define $2\ell \equiv |\mathbf{T}|$, where $\ell=0.21$ nm and $a \equiv |\mathbf{a}_1|=0.25$ nm. The density of an edge state has a value only on A atoms, which is represented by solid circles. The radius of a solid circle is proportional to the density, which shows the localization. (b) The edge states exist near the zigzag edge $(R^t=0)$ of the $(n,0)$ CNT with open boundary. The diameter and length of the CNT is denoted by d_t and L, respectively. (c) $\mathcal{H}_{\mathrm{nn}}$ has a flat energy band of the edge states between the K and K' points at the Fermi energy $(E_F=0)$. $\mathcal{H}_{\mathrm{nnn}}$ causes a bandwidth $W=\gamma_n$. (d) We plot the localization length, $\xi(k)/\ell = -1/\ln(2|\cos(ka/2)|)$ for $2\pi/3 < ka < 4\pi/3$.

$<4\pi/3)$.[7] The edge state behaves as a plane wave around the axis [R^c in Fig. 1(b)], while wave function is localized in the direction of nanotube axis R^t. The localization length in the direction perpendicular to the edge is k dependent, $\xi(k) = -|\mathbf{T}|/2\ln(2|\cos(ka/2)|)$ [see Fig. 1(d)].[16] Though $\xi(k)$ becomes infinite when $ka \to 2\pi/3$ or $ka \to 4\pi/3$ for a graphene, we can show that $\xi(k) \lesssim d_t/2$ for a CNT, where $d_t \equiv na/\pi$ is the diameter of the zigzag CNT. To explain this, let us consider a metallic zigzag CNT, $(3m,0)$. Then, k for the edge states are discrete due to the periodic boundary condition, which is given by $k(i)=2\pi/3a+2\pi i/3ma$ $(i =1,\ldots,m-1)$. We get the largest localization length $\xi(k(1))=\xi(k(m-1))\approx d_t/2$.

The wave function of the edge state is written as[7]

$$|\Psi_k\rangle = \frac{N_k}{\sqrt{n}}\sum_u \exp\left\{ikR^c_{u,A} - \frac{R^t_{u,A}}{\xi(k)}\right\}|\phi(\mathbf{R}_{u,A})\rangle, \qquad (1)$$

where $|\phi(\mathbf{R}_{u,s})\rangle$ is $2p_z$ orbital of a carbon atom and N_k is a normalization constant. The summation on u is taken for all unit cells of graphene or a CNT. We take the coordinate $\mathbf{R}=(R^c,R^t)$ on the cylindrical surface of a zigzag CNT, in which R^c and R^t are coordinates around and along the tube axis, respectively [Fig. 1(b)]. The position of a carbon atom is denoted by $\mathbf{R}_p \equiv (R^c_{u,s},R^t_{u,s})$, where $p=(u,s)$ represents the

sth sublattice ($s=A,B$) in the uth hexagonal unit cell. As is taken for the zigzag edge site $R_{u,A}^t=0$, the edge state has amplitudes only on A atoms ($s=A$). Equation (1) is correct for $2\pi/3 < ka \le \pi$. For $\pi < ka < 4\pi/3$, a phase factor $\exp\{i\pi R_{u,A}^t/\ell\}$ should be multiplied to $|\phi(\mathbf{R}_{u,A})\rangle$.[16]

B. Electron-phonon interaction

The el-ph interaction for graphene is formulated by Jiang et al.,[9] which will be applied to the edge states. The el-ph interaction for the edge states is written as

$$\mathcal{H}_{\text{int}} = \frac{1}{\sqrt{N_u}}\sum_{k,k'}\sum_{q_t,\nu}\alpha_{kk'}^{\nu}(\mathbf{q})(b_{\mathbf{q},\nu}+b_{-\mathbf{q},\nu}^{\dagger})c_{k'}^{\dagger}c_k, \quad (2)$$

where N_u is the number of graphite unit cells, c_k is the annihilation operator of the edge state, and $b_{\mathbf{q},\nu}$ is the annihilation operator of the νth phonon mode. There are six phonon modes: out-of-plane tangential acoustic (optical) mode [oTA (oTO)], in-plane tangential acoustic (optical) mode [iTA (iTO)], and longitudinal acoustic (optical) mode [LA (LO)].[17] $\alpha_{kk'}^{\nu}(\mathbf{q})$ is the el-ph interaction connecting two edge states k and k' by νth phonon mode with momentum $\mathbf{q}$. Due to the momentum conservation along the edge, $k'=k+q$, while the wave vector perpendicular to the edge q_t is needed to sum over the Brillouin zone. $\alpha_{kk'}^{\nu}(\mathbf{q})$ is given by $\alpha_{kk'}^{\nu}(\mathbf{q})\equiv A^{\nu}(\mathbf{q})M_{kk'}^{\nu}(\mathbf{q})/\sqrt{2}$ where $A^{\nu}(\mathbf{q})=\sqrt{\hbar/m_c\omega_\nu(\mathbf{q})}$ is the amplitude of phonon [$\hbar\omega_\nu(\mathbf{q})$ is the energy of the νth phonon with the momentum $\mathbf{q}$] and $M_{kk'}^{\nu}(\mathbf{q})$ is the el-ph matrix element,

$$M_{kk'}^{\nu}(\mathbf{q}) \equiv -\sum_p \langle\Psi_{k'}|\nabla v(\mathbf{R}_p)|\Psi_k\rangle\cdot U(\mathbf{R}_p)\mathbf{e}_{\mathbf{q}}^{\nu}(s)e^{i\mathbf{q}\cdot\mathbf{R}_p}. \quad (3)$$

Here, $v(\mathbf{R}_p)$ is the Kohn-Sham potential of a neutral pseudoatom calculated on the basis of density-functional theory by Porezag et al.[8] for a carbon atom at $\mathbf{R}_p$, $\mathbf{e}_{\mathbf{q}}^{\nu}(s)$ is phonon eigenvector at an s atom normalized in the unit cell as $\Sigma_{s=A,B}\mathbf{e}_{\mathbf{q}}^{\nu}(s)^*\cdot\mathbf{e}_{\mathbf{q}}^{\nu}(s)=1$, and $U(\mathbf{R}_p)$ is a rotational operator for $\mathbf{e}_{\mathbf{q}}^{\nu}(s)$ from an sth atom at origin to a sth atom at $\mathbf{R}_p$. To obtain $\omega_\nu(\mathbf{q})$ and $\mathbf{e}_{\mathbf{q}}^{\nu}(s)$, we use the force constant parameters calculated by Dubay and Kresse[18] for the dynamical matrix.[17]

Putting Eq. (1) into Eq. (3), we obtain

$$M_{kk'}^{\nu}(\mathbf{q}) = -\frac{N_{k'}N_k}{n}\sum_{u',u}\exp\left\{-ik'R_{u',A}^c+ikR_{u,A}^c-\frac{R_{u',A}^t}{\xi(k')}\right. $$
$$\left.-\frac{R_{u,A}^t}{\xi(k)}\right\}m(\mathbf{R}_{u',A},\mathbf{R}_{u,A};\mathbf{q},\nu), \quad (4)$$

where $m(\mathbf{R}_{u',A},\mathbf{R}_{u,A};\mathbf{q},\nu)$ is the atomic deformation potential [9] defined by

$$m(\mathbf{R}_{u',A},\mathbf{R}_{u,A};\mathbf{q},\nu) \equiv \sum_p \langle\phi(\mathbf{R}_{u',A})|\nabla v(\mathbf{R}_p) $$
$$\times|\phi(\mathbf{R}_{u,A})\rangle\cdot U(\mathbf{R}_p)\mathbf{e}_{\mathbf{q}}^{\nu}(s)e^{i\mathbf{q}\cdot\mathbf{R}_p}. \quad (5)$$

There are two types of $m(\mathbf{R}_{u',s'},\mathbf{R}_{u,s};\mathbf{q},\nu)$. The first type is

the case of $(u',s')=(u,s)$ which is referred to as the *on-site* atomic deformation potential.[9] The other one is $(u',s')\ne(u,s)$ which is the *off-site* atomic deformation potential. The on-site (off-site) atomic deformation potential represents a scattering process of an electron from $\mathbf{R}_{u,s}$ to the same (a different) site.

The off-site deformation potential matrix element for the next-nearest A atoms, $|\langle\phi(\mathbf{R}_{u',A})|\nabla v(\mathbf{R}_p)|\phi(\mathbf{R}_{u,A})\rangle\cdot\hat{n}|$, is negligible (for any $\mathbf{R}_p$) in Eq. (5) because it decays quickly as a function of $|\mathbf{R}_{u',A}-\mathbf{R}_{u',A}|$, where $\hat{n}$ is a unit vector along the two carbon atoms. Density-functional theory gives that the off-site deformation potential matrix element for nearest-neighbor interaction is $|\langle\phi(\mathbf{R}_{u,B})|\nabla v(\mathbf{R}_{u,B})|\phi(\mathbf{R}_{u,A})\rangle\cdot\hat{n}|$ ~3 eV/Å.[8,9] As we pointed out above, the wave function of the edge state has an amplitude only of one sublattice and thus this nearest-neighbor term does not contribute to $\alpha_{kk'}^{\nu}(\mathbf{q})$. Thus the off-site atomic deformation potential does not contribute to $\alpha_{kk'}^{\nu}(\mathbf{q})$ for the edge states. For the on-site atomic deformation potential, we need to consider several carbon atoms which are located near $\mathbf{R}_{u,A}$ for the center of deformation potential $\mathbf{R}_p$ in Eq. (5). The value of $|\langle\phi(\mathbf{R}_{u,A})|\nabla v(\mathbf{R}_p)|\phi(\mathbf{R}_{u,A})\rangle\cdot\hat{n}|$ is not negligible if $|\mathbf{R}_p-\mathbf{R}_{u,A}|$ ≤3 Å. Density-functional theory gives that the largest contribution from nearest-neighbor site is $|\langle\phi(\mathbf{R}_{u,A})|\nabla v(\mathbf{R}_{u,B})|\phi(\mathbf{R}_{u,A})\rangle\cdot\hat{n}|\sim8$ eV/Å.[8] Thus, on-site deformation potential is more important than the off-site deformation potential.[10]

Now, we can write $m(\mathbf{R}_{u',A},\mathbf{R}_{u,A};\mathbf{q},\nu)$ as

$$m(\mathbf{R}_{u',A},\mathbf{R}_{u,A};\mathbf{q},\nu) = \delta_{u'u}m_{\text{on}}(R_{u,A}^t;\mathbf{q},\nu)e^{i\mathbf{q}\cdot\mathbf{R}_{u,A}}, \quad (6)$$

where $m_{\text{on}}(R_{u,A}^t;\mathbf{q},\nu)$ is on-site deformation potential from all possible $\mathbf{R}_p$ defined as

$$m_{\text{on}}(R_{u,A}^t;\mathbf{q},\nu) \equiv \sum_p \langle\phi(\mathbf{R}_{u,A})|\nabla v(\mathbf{R}_p) $$
$$\times|\phi(\mathbf{R}_{u,A})\rangle\cdot U(\mathbf{R}_p)\mathbf{e}_{\mathbf{q}}^{\nu}(s)e^{i\mathbf{q}\cdot(\mathbf{R}_p-\mathbf{R}_{u,A})}.(7)$$

Putting Eq. (6) into Eq. (4), we get

$$M_{kk'}^{\nu}(\mathbf{q}) = -N_{k'}N_k\delta_{k',k+q}\sum_{R_{u,A}^t}\exp\left\{\left(iq_t-\frac{1}{\xi(k')}\right.\right. $$
$$\left.\left.-\frac{1}{\xi(k)}\right)R_{u,A}^t\right\}m_{\text{on}}(R_{u,A}^t;\mathbf{q},\nu). \quad (8)$$

For $ka\le\pi<k'a$ or $k'a\le\pi<ka$, we must multiply $\exp\{i\pi R_{u,A}^t/\ell\}$ to $m_{\text{on}}(R_{u,A}^t;\mathbf{q},\nu)$ in Eq. (8).

It is noted that $m_{\text{on}}(R_{u,A}^t;\mathbf{q},\nu)$ is defined to be independent of $R_{u,A}^c$. Instead, $R_{u,A}^c$ appears in the phase of $m(\mathbf{R}_{u,A},\mathbf{R}_{u,A};\mathbf{q},\nu)$ in Eq. (6). The phase gives the momentum conservation around the tube axis, $\delta_{k',k+q}$, after the summation about $R_{u,A}^c$ is made in Eq. (4). On the other hand, $m_{\text{on}}(R_{u,A}^t;\mathbf{q},\nu)$ depends on $R_{u,A}^t$ because Σ_p in Eq. (7) is restricted for $R_p^t\ge0$ and $m_{\text{on}}(R_{u,A}^t;\mathbf{q},\nu)$ does not have a translational symmetry near the edge. Hereafter, we refer $m_{\text{on}}(R_{u,A}^t;\mathbf{q},\nu)$ as the boundary deformation potential.

$m_{\text{on}}(R_{u,A}^t;\mathbf{q},\nu)$ depends on ν strongly. The iTO and LO modes whose eigenvectors are pointing in the direction per-

(a)   (b)

$$\mathbf{e}_0^{\mathrm{oTA}}(A) \quad U(\mathbf{R}_p)\mathbf{e}_0^{\mathrm{oTA}}(A)$$

$$(U(\mathbf{R}_p) - E)\mathbf{e}_0^{\mathrm{oTA}}(A)$$

relative vector

$$\mathbf{R}_{u,A} \quad \mathbf{R}_p$$ $$\mathbf{R}_{u,A} \quad \mathbf{R}_p$$
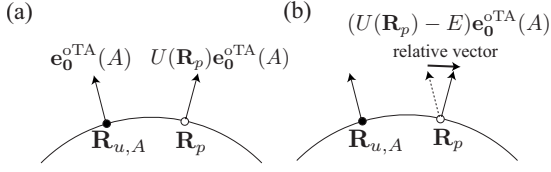
FIG. 2. (a) For the oTA mode with $\mathbf{q}=\mathbf{0}$, the eigenvectors of two atoms at $\mathbf{R}_{u,A}$ and $\mathbf{R}_p$ are pointing perpendicular to the CNT surface. (b) In order to calculate the atomic deformation potential, one needs to consider the relative displacement of two carbon atoms.

pendicular to the edge give a large contribution to $m_{\mathrm{on}}(R_{u,A}^t;\mathbf{q},\nu)$. We generally expect that the boundary deformation potential appears only near the edge. In fact, $|\langle\phi(\mathbf{R}_{u,A})|\nabla v(\mathbf{R}_p)|\phi(\mathbf{R}_{u,A})\rangle\cdot\hat{n}|$ is finite only when $|\mathbf{R}_p-\mathbf{R}_{u,A}| \lesssim 3$ Å. Thus, $m_{\mathrm{on}}(R_{u,A}^t;\mathbf{q},\nu)$ depends on $R_{u,A}^t$ only when $R_{u,A}^t \lesssim 3$ Å. The boundary deformation potential contributes to the matrix element increasingly with decreasing $\xi(k)$ or $\xi(k')$, which can be seen in Eq. (8).

In Eq. (7), we must consider relative atomic motion of $\mathbf{R}_{u,A}$ to $\mathbf{R}_p$. This can be done by replacing $U(\mathbf{R}_p)$ with $U(\mathbf{R}_p)-E$, where E is the unit matrix. In Fig. 2(a), we show phonon eigenvector of the oTA mode pointing perpendicular to the nanotube surface. If we consider the phonon eigenvector in a flat surface or graphene, the relative displacement of the two atoms becomes zero when $\mathbf{q}=\mathbf{0}$. However, it is not the case for a cylindrical surface. As shown in Fig. 2(b), the relative eigenvector, $[U(\mathbf{R}_p)-E]\mathbf{e}_q^{\mathrm{oTA}}(s)$, remains finite. The relative vector for the oTA mode changes the area on a cylindrical surface and is similar to the LA mode except for a $1/d_t$ reduction of the amplitude, by which $m_{\mathrm{on}}(R_{u,A}^t;\mathbf{q},\mathrm{oTA})$ is proportional to $1/d_t$. On the other hand, the relative displacement becomes zero for the in-plane modes such as iTA and LA when $\mathbf{q}\to\mathbf{0}$. Thus, the el-ph interaction by the iTA and LA modes vanish for $\mathbf{q}=\mathbf{0}$, while the oTA mode provides a finite $m_{\mathrm{on}}(R_{u,A}^t;\mathbf{q},\mathrm{oTA})$ even for $\mathbf{q}=\mathbf{0}$. Hereafter, we simply use $U(\mathbf{R}_p)$ for $U(\mathbf{R}_p)-E$.

III. CALCULATED RESULTS

In this section, we plot $|M_{kk'}^{\nu}(\mathbf{q})|$ for several values of k and k' and examine the dependence of $|M_{kk'}^{\nu}(\mathbf{q})|$ on phonon mode ν in Sec. III A and on nanotube diameter d_t in Sec. III B.

A. ν dependence of $|M_{kk'}^{\nu}(\mathbf{q})|$

In the calculation, we consider the magnitude of $M_{kk'}^{\nu}(\mathbf{q})$ for the (60, 0) CNT ($d_t\approx 5$ nm). In Fig. 3, we plot $|M_{kk'}^{\nu}(\mathbf{q})|$ as a function of q_t for (a) $(k,k')=(7\pi/10,8\pi/10)$ and (b) $(26\pi/30,29\pi/30)$. The corresponding phonon eigenvector is the same ($q=\pi/10$). Thus, the difference between the two cases shows the dependence of $|M_{kk'}^{\nu}(\mathbf{q})|$ on $\xi(k)$ and $\xi(k')$. $(7\pi/10,8\pi/10)$ is chosen as an example that $\xi(k)$ (=22 Å) and $\xi(k')$ (=4.4 Å) are longer than the carbon-carbon bond length ($a_{\mathrm{cc}}=1.4$ Å), while $(26\pi/30,29\pi/30)$ is chosen as an

(a) $(k,k') = (7\pi/10, 8\pi/10)$ (b) $(k,k') = (26\pi/30, 29\pi/30)$
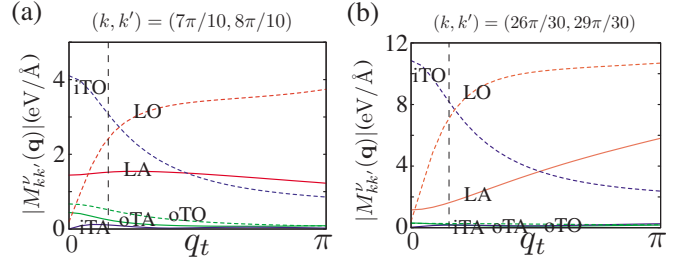
FIG. 3. (Color online) $|M_{kk'}^{\nu}(\mathbf{q})|$ for the (60, 0) zigzag CNT: (a) $(k,k')=(7\pi/10,8\pi/10)$ and (b) $(k,k')=(26\pi/30,29\pi/30)$ are plotted as a function of q_t, where $q=\pi/10$. Three solid curves represent acoustic phonon modes, oTA (green), iTA (blue), and LA (red), and three dashed curves are optical modes, oTO (green), iTO (blue), and LO (red). The vertical dashed lines represent $q_t=\sqrt{3}q$ ($\sqrt{3}=|\mathbf{T}|/|\mathbf{a}_1|$).

example that $\xi(k)$ (=2.4 Å) and $\xi(k')$ (=0.9 Å) are comparable to a_{cc}.

As shown in Fig. 3(a), $|M_{kk'}^{\mathrm{iTO}}(\mathbf{q})|$ is 4 eV/Å at $q_t=0$. $|M_{kk'}^{\mathrm{LO}}(\mathbf{q})|$ decreases with increasing q_t, while $|M_{kk'}^{\mathrm{LO}}(\mathbf{q})|$ increases with increasing q_t. This behavior of the iTO and LO modes relates to the boundary deformation potential. The eigenvector of the iTO (LO) mode is pointing along the tube axis when $q_t/|\mathbf{T}|<q/|\mathbf{a}_1|$ ($q_t/|\mathbf{T}|>q/|\mathbf{a}_1|$) and then produces a large boundary deformation potential. On the other hand, $\mathbf{e}_q^{\mathrm{oTO}}(s)$ is perpendicular to the CNT axis and the oTO mode does not contribute to a boundary deformation potential. The value of $|M_{kk'}^{\mathrm{oTO}}(\mathbf{q})|$ is considerably smaller than $|M_{kk'}^{\nu}(\mathbf{q})|$ for the iTO and LO modes. Thus, the contribution of the oTO mode to the el-ph interaction can be neglected for $d_t \approx 5$ nm CNT. In Fig. 3(b), $|M_{kk'}^{\mathrm{iTO}}(\mathbf{q})|$ and $|M_{kk'}^{\mathrm{LO}}(\mathbf{q})|$ reach 11 eV/Å, which indicates that $|M_{kk'}^{\nu}(\mathbf{q})|$ for the iTO and LO modes increase significantly with decreasing $\xi(k)$ and $\xi(k')$. The boundary deformation potential becomes more effective with decreasing the localization length.

The matrix element for iTA mode is smaller than the other acoustic modes for a wide range of q_t as shown in Fig. 3(a). Though $|M_{kk'}^{\mathrm{iTA}}(\mathbf{q})|$ can be comparable to $|M_{kk'}^{\mathrm{oTA}}(\mathbf{q})|$ as shown in Fig. 3(b), the contribution of the iTA mode to the el-ph interaction is negligible to that for oTA because the amplitude of the iTA mode is smaller than that of the oTA mode; $A^{\mathrm{iTA}}(\mathbf{q})\lesssim A^{\mathrm{oTA}}(\mathbf{q})$. On the other hand, the oTA and LA modes are important for lower temperature in the el-ph interaction. The oTA mode changes the volume of a CNT and gives an on-site deformation potential as shown in Fig. 2. Moreover, the energy of the oTA mode is the smallest among acoustic modes and thus $A^{\mathrm{oTA}}(\mathbf{q})$ can be larger than $A^{\mathrm{LA}}(\mathbf{q})$. The LA mode is a area-changing mode and produces a large on-site deformation potential and contributes to the matrix element most significantly among acoustic modes.

B. d_t dependence of $|M_{kk'}^{\nu}(\mathbf{q})|$

It is shown from Eq. (8) that $M_{kk'}^{\nu}(\mathbf{q})$ for two CNTs with different diameters (d_t) are the same for the same values of k and k'. In general, we can find the similar values of k (or k')
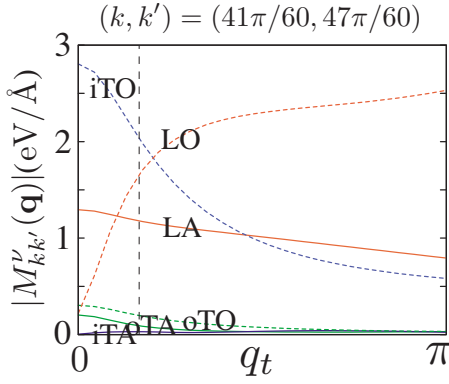
FIG. 4. (Color online) $|M_{kk'}^{\nu}(\mathbf{q})|$ for (120,0) zigzag CNT. The phonon eigenvector is the same as in Fig. 3. The vertical dashed line represents $q_t = \sqrt{3}q$.

for different d_t. However, it is not the case for edge states near the K or K' point. Then, $M_{kk'}^{\nu}(\mathbf{q})$ depends on d_t for such edge states. For instance, $M_{kk'}^{\nu}(\mathbf{q})$ depends on d_t for the largest $\xi(k) \approx d_t/2$. In Fig. 4, we plot $|M_{kk'}^{\nu}(\mathbf{q})|$ for $(41\pi/60, 47\pi/60)$ of the (120, 0) CNT ($d_t \approx 10$ nm). The $|M_{kk'}^{\nu}(\mathbf{q})|$ has the similar functional shape to that in Fig. 3(a) while the values become smaller.

The reduction of $|M_{kk'}^{\nu}(\mathbf{q})|$ can be explained as follows. If we neglect the d_t dependence of the boundary deformation potential, the summation on $R_{u,A}^t$ in Eq. (8) can be performed analytically. $M_{kk'}^{\nu}(q_t=0)$ is then proportional to the factor $R_{kk'}(d_t)$,

$$R_{kk'}(d_t) \equiv \frac{\sqrt{\xi(k)\xi(k')}}{\xi(k)+\xi(k')}, \qquad (9)$$

where $R_{kk'}(d_t)$ is a function of d_t because ξ depends on d_t. Since $R_{kk'}(5 \text{ nm})=0.37$ and $R_{kk'}(10 \text{ nm})=0.30$, we have $R_{kk'}(10 \text{ nm})/R_{kk'}(5 \text{ nm}) \approx 0.81$. This ratio reproduces $|M_{kk'}^{LA}(\mathbf{q})|_{10 \text{ nm}}/|M_{kk'}^{LA}(\mathbf{q})|_{5 \text{ nm}}=1.3/1.5 \approx 0.86$ at $q_t=0$.

IV. LOCAL DENSITY OF STATES

Now, we calculate a renormalized energy dispersion relation and LDOS using self-energy $\Sigma(k,i\omega_n)$ which is defined by

$$\Sigma(k,i\omega_n) = \frac{2k_B T}{N_u} \sum_m \sum_{\mathbf{q},\nu} \frac{|\alpha_{kk+q}^{\nu}(\mathbf{q})|^2 \hbar\omega_\nu(\mathbf{q})}{(\omega_n-\omega_m)^2+[\hbar\omega_\nu(\mathbf{q})]^2}$$
$$\times \frac{1}{i\omega_m - [E(k+q)-E_F] - \Sigma(k+q,i\omega_m)}, \qquad (10)$$

where T is temperature and $\omega_n=\pi k_B T(2n+1)$ is the Matsubara frequency (n is an integer). We put the cutoff Matsubara frequency $|\omega_n| \lesssim \hbar\omega_D \approx 0.2$ eV. By means of Padé approximation,[19] $\Sigma(k,i\omega_n)$ is changed to that on the real axis of ω: $\Sigma(k,\omega)$. Then, we find a solution ϵ satisfying $\epsilon = [E(k)-E_F] + \text{Re}(\Sigma(k,\epsilon))$ as a function of k, E_F, and T. The
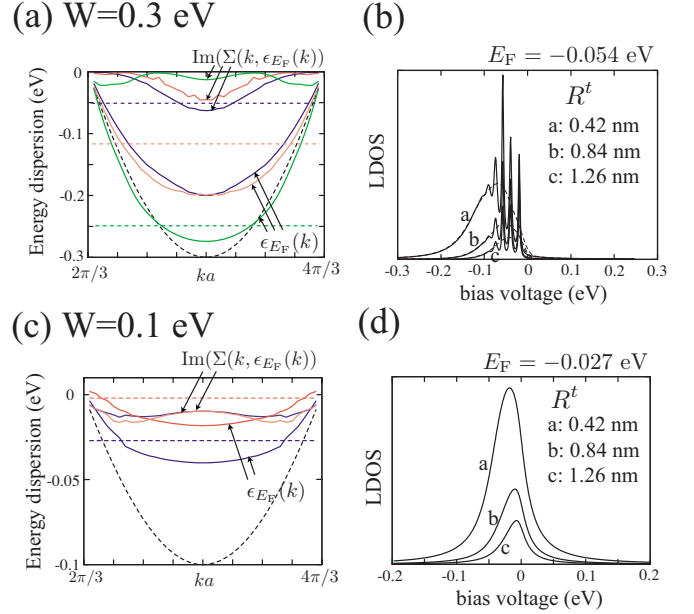
FIG. 5. (Color online) Calculated energy dispersion $\epsilon_{E_F}(k)$ and LDOS $D(V,R^t)$ for [(a) and (b)] $W=0.3$ eV and [(c) and (d)] $W=0.1$ eV. In (a), $E(k)$ is plotted as the dashed curve, and $\epsilon_{E_F}(k)$ is plotted for $E_F=-0.054$, -0.122, and -0.250 eV. We plot $\text{Im}(\Sigma(k,\epsilon_{E_F}(k)))$ to show the k dependence. In (b), $D(V,R^t)$ for $E_F=-0.054$ eV and its smoothed curve (dashed curve) are plotted for $R^t=0.42$, 0.84, and 1.26 nm. In (c), $\epsilon_{E_F}(k)$ is plotted for $E_F=-0.002$ and -0.027 eV. In (d), we plot $D(V,R^t)$ for $E_F=-0.027$ eV.

obtained $\epsilon_{E_F,T}(k)$ is a renormalized energy dispersion relation. We adopt $T=50$ K in the following calculations. The T dependence of $\epsilon_{E_F,T}(k)$ is negligible for a wide range of T, for instance, $T=77$ K gives almost the same result. Calculations at low temperature have some numerical advantages since the number of ω_n increases. The LDOS curve is defined as a function of bias voltage (V) between graphene and the STS tip, and the distance (R^t) from the zigzag edge sites and the STS tip by

$$D(V,R^t) = \frac{1}{\pi}\sum_k \frac{\Gamma_{E_F}(k)/2}{[V-\epsilon_{E_F}(k)]^2+[\Gamma_{E_F}(k)/2]^2}|\Psi_k(R^t)|^2, \qquad (11)$$

where $\Gamma_{E_F}(k) \equiv -2\,\text{Im}(\Sigma(k,\epsilon_{E_F}(k)))$ is the width of STS spectrum. It is noted that the value of E_F is given in such a way that the number of edge states below E_F is conserved when we calculate $\Sigma(k,i\omega_n)$ self-consistently, that is, $\Sigma_{E(k)<E_F}1 = \Sigma_{\epsilon_{E_F}(k)<E_F}1$.

Numerical result

In Fig. 5(a), we plot $E(k)$ ($W=0.3$ eV) without self-energy correction as the dashed curve and renormalized energy dispersion $\epsilon_{E_F}(k)$ for $E_F=-0.054$, -0.122, and -0.250 eV as the blue, red, and green curves, respectively. The reason why we consider different E_F values is that in the experiment, charge transfer from STS tip or substrate may modify the E_F values

and that we need to investigate E_F dependence. The parallel dashed lines denote the Fermi level for these E_F values. For each value of E_F, $\mathrm{Im}(\Sigma(k, \epsilon_{E_F}(k)))$ is plotted to show the k dependence. By denoting the renormalized bandwidth as W', we obtain $W' \approx 0.2$ eV for $E_F = -0.054$ and -0.122 eV. The corresponding mass enhancement parameter λ is about 0.5, where we defined $\lambda = W/W' - 1$. When $E_F = -0.250$ eV, W' is about 0.27 eV and $\lambda \approx 0.1$. We observe that the value of $\Gamma_{E_F}(ka = \pi)$ is about 0.13 eV when $E_F = -0.054$ eV. The calculated $\epsilon_{E_F}(k)$ and $\mathrm{Im}(\Sigma(k, \epsilon_{E_F}(k)))$ strongly depend on the value of E_F.

The values of W' and $\Gamma_{E_F}(k)$ relate to the peak position and width of $D(V, R^t)$. We plot $D(V, R^t)$ for $E_F = -0.054$ eV at $R^t = 0.42$, 0.84, and 1.26 nm in Fig. 5(b). The LDOS curves have several sharp spikes at $V = \epsilon_{E_F}(k)$ due to relatively small value of $\Gamma_{E_F}(k)$ compared with the finite level spacing of the edge states. Here, we take (120,0) CNT ($d_t \approx 10$ nm) for calculating the self-energy. For a graphene ($d_t \to \infty$), the level spacing becomes zero and the spike structure will disappear. The calculated LDOS structure for $E_F = -0.054$ eV has a peak near $V \approx -60$ meV, which is close to the observed LDOS in which a peak is located at $V = -30$ to -20 meV.[2–5] However, the width of the peak is about 0.7 eV, which is much larger than the experiment[2,4] (0.05–0.1 eV). The peak position and the width are improved to fit the experimental data when $W = 0.1$ eV, as shown in Figs. 5(c) and 5(d). In this case, $W' = 0.02$ and 0.04 for $E_F = -0.002$ and -0.27 eV, respectively. The calculated LDOS structure for $E_F = -0.027$ eV has a peak near $V \approx -20$ meV, with the width of ≈ 0.05 eV. The small value of W does not show any spike structure due to the discrete k values. Thus, overall feature seems to be better for $W = 0.1$ eV than $W = 0.3$ eV. It should be noted that $W = 0.1$ eV is not always consistent with the experiment. When we assume that all the edge states are below the Fermi energy, we see that E_F appears above $E = 0$ eV, which gives a peak very close or above the $V = 0$ eV, while the experiment shows $V = -30$ to -20 meV.

It is worth mentioning that Niimi *et al.*[2,3] reported that the tunnel current was unstable when the STS tip was located very close to the zigzag edge. Then, the electron injected from the STS tip has a large transition amplitude to edge states having $\xi(k) < 2\ell$ (0.42 nm), that is, k states which are around $ka = \pi$ state [see Fig. 1(d)]. As shown in Fig. 5(c), the magnitude of $\Gamma_{E_F}(k)$ is much larger than $k_B T$ (≈ 0.0045 eV) for most value of k, and $\Gamma_{E_F}(k)$ for states around $ka = \pi$ state reaches about 0.02 eV and yields strong fluctuation. It indicates that the tunnel current is unstable. We calculate $D(V, 0)$ and find that the height and width of the peak are both significantly larger (more than ten times larger) than $D(V, R^t)$ for $R^t = 0.42$ nm. As we noted in Sec. II, iTO and LO modes give a large matrix element through the boundary deformation potential. The boundary deformation potential may be relevant to the unstable tunnel current. Since the injected electron from a STS tip is localized near the edge, we expect that the tunnel current would be strongly affected by the boundary deformation potential.

V. DISCUSSION AND SUMMARY

We showed that el-ph interaction for edge states consists only of the on-site atomic deformation potential. As a result, LA mode contributes to the scattering most effectively and the on-site deformation potential is enhanced at the edge for LO and iTO modes. It is to be noted that the on-site atomic deformation potential does not contribute to backward scattering of extended states and the off-site atomic deformation potential gives rise to resistivity.[10] Because the on-site atomic deformation potential is larger than the off-site atomic deformation potential, the edge states exhibit the strong el-ph coupling character that the graphite system originally possesses.

The original energy bandwidth of the edge states, W, is consistent with the observed position of LDOS peak when $W \approx 0.1$ eV, which is the same order of $\gamma_n \approx 0.3$ eV but not the same value. It is noted that the case of $W = 0.3$ eV does not include the overlapping integral (s parameter[17]) which increases (decreases) the conduction (valence) bandwidth. To examine the effect of s parameter on the bandwidth of the edge states, we performed the energy band structure calculation in an extended tight-binding framework[20] and obtained $W \approx 0.2$ eV. We expect that W is externally modified by attaching a functional group or contacting an electrode to the edge sites.

Our calculation of the el-ph interaction does not have any adjustable parameters. It is noted that the pseudopotential[8] adopted in the present paper is used for calculating resonance Raman intensity in which the calculated results explain chirality and diameter dependence of the Raman intensity quantitatively.[9] However, we did not take into account electron-electron (el-el) interaction in our calculations, which can lead to changes of our results. The effect of el-el interaction warrants future work concerning the details of LDOS curve. At the present moment, we image that the repulsive on-site U affects not the energy bandwidth but the relative position of energy subbands for up and down spins which may make a magnetic behavior. Detailed experimental data of STM/STS for zigzag edge of CNTs and graphene may be useful for a qualitative estimation of the strength of the el-el interaction. When the values of W and $\hbar \omega_D$ are comparable, the vertex correction may be important since the Migdal theorem is not applicable. Although our results are consistent with the STS data, it is possible that vertex correction may change $\alpha^{\nu}_{kk'}(\mathbf{q})$. However, the vertex correction to $\alpha^{\nu}_{kk'}(\mathbf{q})$ is beyond our scope of the present paper.

We did not consider the el-ph matrix element between extended state and edge state. Although the matrix element may be enhanced by the boundary deformation potential, it is naively expected that the matrix element is proportional to $\sqrt{\xi/L}$ and is negligible when $L \gg \xi$. In this case, the extended state and the edge state are decoupled. The geometry with $d_t \gg L$ is referred to as the nanographite ribbon. For a ribbon, the off-site atomic deformation potential contributes to the scattering between two edge states which are located at the different edges, since overlapping between the two edge states is not negligible. It is noted that Igami *et al.*[21] showed that out-of-plane edge phonon modes appear depending on

the effective mass of carbon atom at edge sites, and Tanaka *et al.*[22] observed such modes at the armchair edge of nanographite ribbons on TiC(755) surface by high resolution electron energy loss spectroscopy. Though $e_q^\nu(s)$ and $\omega_\nu(\mathbf{q})$ used in this paper do not include the edge phonon mode, el-ph coupling for out-of-plane modes is negligible for the edge states. The el-ph interaction for nanoribbon requires further studies on the el-ph interaction.

We have studied a single graphene sheet with zigzag edges and compared the calculated results with the STS experiments which were performed near step edges at the surface of three-dimensional (3D) graphite.[2–4] For the surface of 3D graphite, however, interlayer interaction is not negligible. For example, STM experiments on graphite surfaces show that there are significant differences between a 3D graphite and graphene. That is, the STM measurements for graphene are unable to see the image for one of the two sublattices of graphite on the surface, which is usually observed for 3D graphite. The appearance of one sublattice in the STM for 3D graphite arises from the interlayer interaction since the one sublattice without an atom in the neighbor layer has a large density of states at the Fermi energy.[23] The present calculation does not consider the interlayer interaction for simplicity, which may explain the difference of two STM images for zigzag edges in the experiment. When we consider a zigzag edge on 3D graphite surface, two possible structures of the zigzag edge, α and β, exist depending on the existence of a carbon atom in the nearest neighbor layer below the edge carbon atom.[5] However, when we see the STS for zigzag edge, the STS experiment does not observe the difference in the spectra between α and β zigzag edges. Thus, we think that the interlayer interaction does not significantly affect the relative position of the edge states to the Fermi energy and the energy bandwidth of the edge states.

In summary, we formulated el-ph interaction for edge states and used it to calculate LDOS. Although our calculation does not include the Coulomb interaction, the result agrees with LDOS data[2–4] when $W \approx 0.1$ eV. Our results should be compared with future experiments on edge states in CNTs and graphene.

*sasaken@flex.phys.tohoku.ac.jp

[1] M. Fujita, K. Wakabayashi, K. Nakada, and K. Kusakabe, J. Phys. Soc. Jpn. **65**, 1920 (1996).

[2] Y. Niimi, T. Matsui, H. Kambara, K. Tagami, M. Tsukada, and H. Fukuyama, Appl. Surf. Sci. **241**, 43 (2005).

[3] Y. Niimi, T. Matsui, H. Kambara, K. Tagami, M. Tsukada, and H. Fukuyama, Phys. Rev. B **73**, 085421 (2006).

[4] Y. Kobayashi, K. I. Fukui, T. Enoki, K. Kusakabe, and Y. Kaburagi, Phys. Rev. B **71**, 193406 (2005).

[5] Y. Kobayashi, K. I. Fukui, T. Enoki, and K. Kusakabe, Phys. Rev. B **73**, 125415 (2006).

[6] K. Sugawara, T. Sato, S. Souma, T. Takahashi, and H. Suematsu, Phys. Rev. B **73**, 045124 (2006).

[7] K. Sasaki, S. Murakami, and R. Saito, Appl. Phys. Lett. **88**, 113110 (2006).

[8] D. Porezag, T. Frauenheim, T. Köhler, G. Seifert, and R. Kaschner, Phys. Rev. B **51**, 12947 (1995).

[9] J. Jiang, R. Saito, G. G. Samsonidze, S. G. Chou, A. Jorio, G. Dresselhaus, and M. S. Dresselhaus, Phys. Rev. B **72**, 235408 (2005).

[10] H. Suzuura and T. Ando, Phys. Rev. B **65**, 235412 (2002).

[11] T. Ando, T. Nakanishi, and R. Saito, J. Phys. Soc. Jpn. **67**, 2857 (1998).

[12] A. Bachtold, M. S. Fuhrer, S. Plyasunov, M. Forero, E. H. Anderson, A. Zettl, and P. L. McEuen, Phys. Rev. Lett. **84**, 6082 (2000).

[13] J.-Y. Park, S. Rosenblatt, Y. Yaish, V. Sazonova, H. Ustunel, S. Braig, T. A. Arias, P. W. Brouwer, and P. L. McEuen, Nano Lett. **4**, 517 (2004).

[14] I. Takesue, J. Haruyama, N. Kobayashi, S. Chiashi, S. Maruyama, T. Sugai, and H. Shinohara, Phys. Rev. Lett. **96**, 057001 (2006).

[15] K. Sasaki, J. Jiang, R. Saito, S. Onari, and Y. Tanaka, J. Phys. Soc. Jpn. **76**, 033702 (2007).

[16] K. Sasaki, S. Murakami, R. Saito, and Y. Kawazoe, Phys. Rev. B **71**, 195401 (2005).

[17] R. Saito, G. Dresselhaus, and M. Dresselhaus, *Physical Properties of Carbon Nanotubes* (Imperial College Press, London, 1998).

[18] O. Dubay and G. Kresse, Phys. Rev. B **67**, 035401 (2003).

[19] H. J. Vidberg and J. W. Serene, J. Low Temp. Phys. **29**, 179 (1977).

[20] G. G. Samsonidze, R. Saito, N. Kobayashi, A. Grüneis, J. Jiang, A. Jorio, S. G. Chou, G. Dresselhaus, and M. S. Dresselhaus, Appl. Phys. Lett. **85**, 5703 (2004).

[21] M. Igami, M. Fujita, and S. Mizuno, Appl. Surf. Sci. **130-132**, 870 (1998).

[22] T. Tanaka, A. Tajima, R. Moriizumi, M. Hosoda, R. Ohno, E. Rokuta, C. Oshima, and S. Otani, Solid State Commun. **123**, 33 (2002).

[23] P. L. Giunta and S. P. Kelty, J. Chem. Phys. **114**, 1807 (2001).